PHYSICAL REVIEW B VOLUME 17, NUMBER 10 15 MAY 1978

Resonance Raman studies in Cu_2O. II. The yellow and green excitonic series

Peter Y. Yu
IBM Thomas J. Watson Research Center, Yorktown Heights, New York 10598

Y. R. Shen
Department of Physics, University of California, and Materials and Molecular Research Division, Lawrence Berkeley Laboratory, Berkeley, California 94720

(Received 28 December 1977)

Resonant Raman scattering of multiphonon modes has been studied in Cu_2O in the region of its yellow and green excitonic series. Resonant enhancements of a large number of Raman modes have been observed. The experimental results have been interpreted quantitatively in terms of three kinds of exciton-phonon scattering processes: (i) intra-yellow-exciton scattering—depending on the energy of the yellow exciton, the phonons involved are the infrared active Γ_{15}^- (660 cm^{-1}) or the Γ_{12}^- (109 cm^{-1}) and Γ_{15}^- (154 cm^{-1}) modes; (ii) interexciton scattering between the $2P$ green exciton state and yellow excitons continuum—the phonon responsible for this scattering process is the high-energy Γ_{15}^- mode; and (iii) intra-green-exciton scattering—only the low-energy Γ_{15}^- mode is involved. From these results a detailed picture of the relaxation mechanisms of the yellow and green excitons in Cu_2O by emission of phonons is obtained.

I. INTRODUCTION

Resonant Raman scattering (RRS) has been studied extensively in Cu_2O because its optical spectra show a large number of excitonic structures associated with electric quadrupole and dipole transitions and phonon-assisted dipole transitions. The enhancement of odd-parity phonons at quadrupole-allowed nS ($n = 1$, 3, 4, and 5) and mD ($m = 3$ and 4) levels of the yellow exciton series in Cu_2O has been studied by Compaan and Cummins,[1] by Genack *et al.*[2] and by Washington *et al.*[3] The higher-energy dipole-allowed blue and violet excitons have been investigated by Yu *et al.*,[4] by Williams and Porto,[5] and by Compaan.[6]

In an earlier paper[7] (hitherto referred to as I) we have reported the RRS at the phonon-assisted $1S$ yellow excitonic absorption edge. In this paper we present our RRS results associated with the dipole-allowed nP states and the continuum states of the yellow and green excitons (part of these results has been published in a short paper[8]). These RRS results provided hitherto unavailable information on the relaxation mechanisms of both the yellow and green excitons.

In Sec. II we briefly review some properties of the yellow and green excitons in Cu_2O which are relevant to this paper but were not covered in I. In Sec. III the experimental results are presented. The data are divided into three groups depending on whether the resonant intermediate state involve only the yellow exciton, only the green exciton, or both. In Sec. IV these experimental results are compared as far as possible with theoretical calculations. In general, good quantitative agreement between theory and experiment is achieved. Finally, Sec. V summarizes our conclusions. In the Appendix, matrix elements of the exciton-LO-phonon (Fröhlich) Hamiltonian are evaluated.

II. OPTICAL PROPERTIES OF THE YELLOW AND GREEN EXCITONS IN Cu_2O

The optical and lattice vibrational properties of Cu_2O have already been reviewed in I. In this paper only those properties of the yellow and green excitons not found in I will be summarized.

The frequencies of the dipole-allowed P states of the yellow and green excitonic series are given, respectively, by[9]:

$$\nu_{Yn} = 17,525 - 786\, n^{-2}\ cm^{-1} \quad (n \geq 2) \tag{1}$$

and

$$\nu_{Gn} = 18,588 - 1242\, n^{-2}\ cm^{-1} \quad (n \geq 2). \tag{2}$$

Figure 1 shows a composite energy-level diagram of the yellow and green excitons in Cu_2O. The positions of the S and D states in the yellow exciton series are taken from the work of Daunois *et al.*[10] and Diess and Daunois.[10] Energies of the S and D states in the green exciton series have not yet been reported. There is still controversy as to the location of some of the S and D levels in the yellow excitonic series (e.g., the $2S$ level).[3] However, for the discussion in the present paper, where these levels are not directly resonant with the incident or scattered photons, these small uncertainties in energies are not significant; so unless otherwise stated we shall assume all the S and D states are degenerate with the corresponding P states.

For convenience we shall use the following notations. The discrete levels in the yellow excitonic

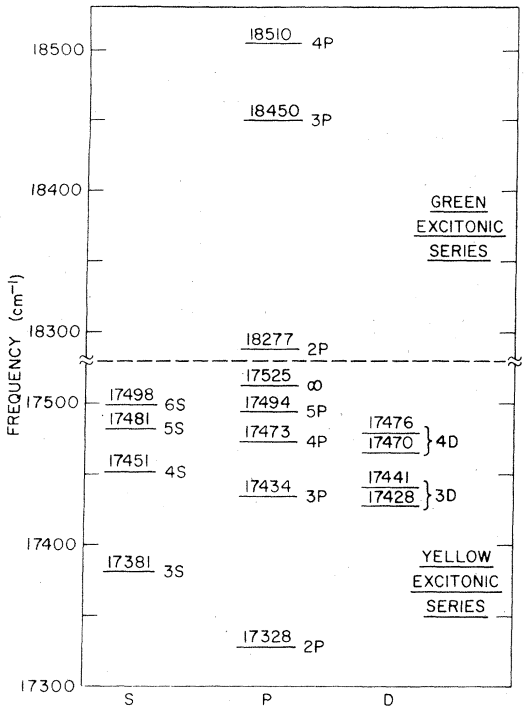

FIG. 1. Energy-level diagram of the yellow and green excitons in Cu_2O. The frequencies of the different levels are obtained from Refs. 3, 10, and 11.

series will be denoted by Y-nS, Y-nP, and Y-nD ($n = 1, 2, 3$, etc.). The energy and damping of the n level will be denoted by $\hbar\omega_{Yn}$ and Γ_{Yn}, respectively. The continuum states of the yellow exciton with energy E will be denoted by Y-EP. In the corresponding notations for the green exciton Y is replaced by G. The two infrared-active longitudinal phonons in Cu_2O, $\Gamma_{15}^{-(1)}$(LO) (154 cm^{-1}) and $\Gamma_{15}^{-(2)}$(LO) (660 cm^{-1}), will be called LO1 and LO2, respectively.

III. EXPERIMENTAL RESULTS

The experimental setup has been described in detail in I and will not be repeated here. In studying photoluminescence in Cu_2O,[11] we found that there are two kinds of Cu_2O crystals: Type I, which shows weak luminescence associated with the Y-1S exciton, and Type II, which shows a luminescence about 50 times stronger. At present this sample dependence of the luminescence intensity of Cu_2O is not understood. Since we have performed most of our previous RRS work on a Type-I sample, for consistency we have also used a Type-I crystal in the present study. However, the results of a limited number of Raman spectra of Type-II samples we have measured indicate that both types of Cu_2O samples show similar resonant

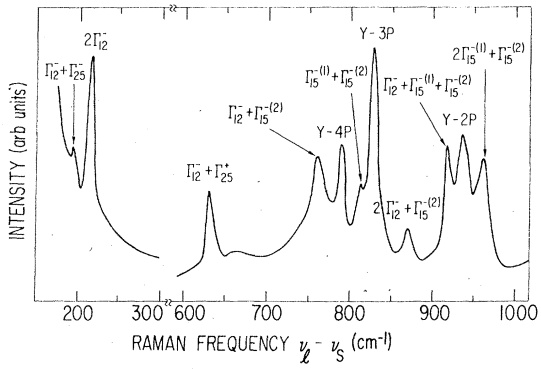

FIG. 2. An emission spectrum of Cu_2O at ~2 °K excited by a dye laser with frequency $\nu_l = 18\,260$ cm^{-1}. The identification of the different peaks is discussed in the text.

enhancement.

Figure 2 shows a typical emission spectrum of Cu_2O when excited by laser radiation with energies in the yellow-exciton continuum. The low-frequency lines at 198 and 220 cm^{-1} have been identified before as $\Gamma_{12}^- + \Gamma_{25}^-$ and $2\Gamma_{12}^-$ Raman modes, respectively.[7] In addition, there is a large number of higher-frequency peaks. To separate the Raman modes from the luminescence peaks we utilize their different dependences on the excitation frequency by plotting the shift of the observed peaks against the excitation frequency.[12] Such a plot is shown in Fig. 3. Points which fall on horizontal straight lines are identified as Raman modes, while points falling on a slanted 45° line are associated with photoluminescence peaks. In this way we found three luminescence peaks in Fig. 2. Since their frequencies coincide with those of Y-2P, Y-3P, and Y-4P, they are identified with rad-

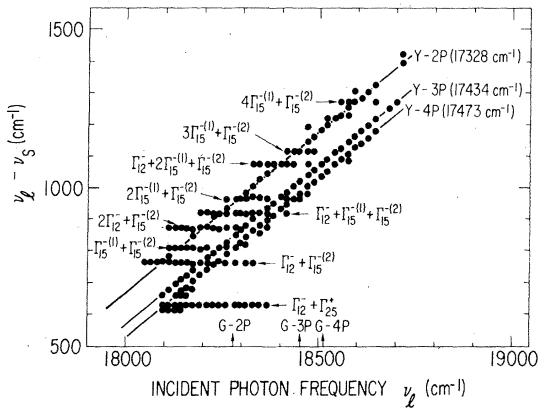

FIG. 3. Raman shift $\nu_l - \nu_s$ of emission peaks of Cu_2O plotted as function of incident photon frequency. The straight lines are drawn corresponding to the Y-2P, Y-3P, and Y-4P luminescence peaks.

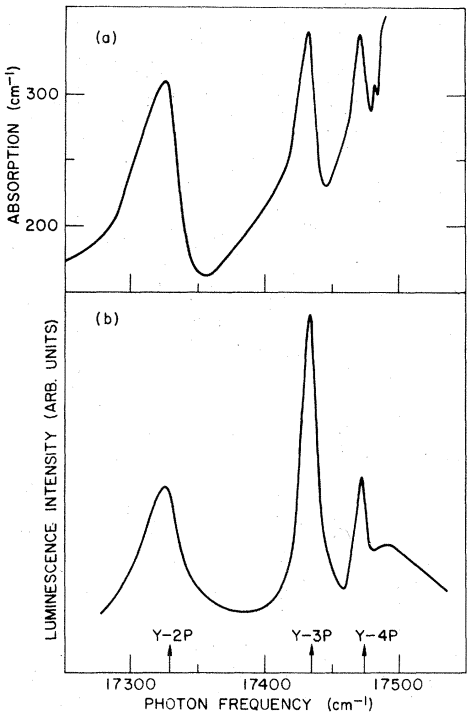

FIG. 4. (a) Absorption and (b) photoluminescence spectra of our Cu_2O sample measured at ~ 2 °K.

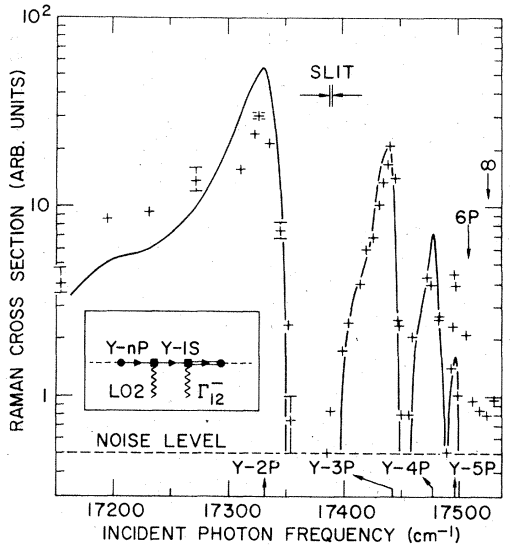

FIG. 5. Raman cross section of the $\Gamma_{12}^- + LO2$ mode of Cu_2O plotted against incident photon frequency in the region of the Y-nP excitons (indicated by arrows). The solid curves are plots of Eq. (9) with one adjustable parameter. The inset is a diagrammatic representation of the scattering process responsible for the observed enhancement of the $\Gamma_{12}^- + LO2$ mode. The notations are: dashed line, photon; single line with arrow, yellow or green exciton; double line with arrow, a dipole-allowed exciton; wiggly line, phonon; ●, exciton-photon Hamiltonian; ■, exciton-phonon Hamiltonian.

iative recombination of these excitons. The photoluminescence spectrum of Cu_2O without interference from Raman peaks is shown in Fig. 4(b). The Raman peaks, on the other hand, can be identified by expressing their Raman frequencies as linear combinations of known zone-center phonon frequencies of Cu_2O which are given in I. Except for the 308 cm^{-1} mode a unique assignment is usually possible. The 308 cm^{-1} peak can be either a 2LO1 or $2\Gamma_{12}^- + \Gamma_{25}^-$ mode. In the range of laser frequencies used in our study, we found the 2LO1 phonon identification more consistent with the strong resonance enhancement shown by this peak.

In general, we found that Raman peaks showing resonance enhancement in the yellow and green exciton regions are combination modes involving only the Γ_{12}^-, LO1, and LO2 phonons. Furthermore, only certain combination of these modes are enhanced at particular laser frequency ranges. Based on where these modes become enhanced, we can conveniently divide our RRS results into three groups.

A. Incident or scattered photons resonant with yellow exciton levels (intra-yellow-exciton scattering)

For incident laser frequency ν_l, resonant with the Y-nP series, only the $\Gamma_{12}^- + LO2$ mode is en-

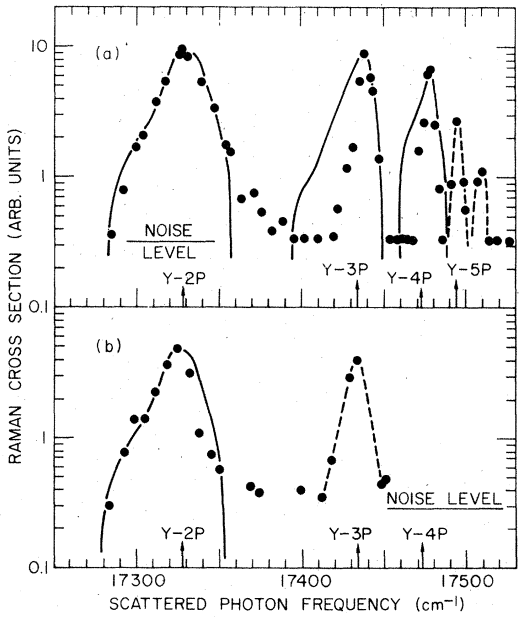

FIG. 6. Raman cross section of the (a) 2LO1 mode and (b) LO1 + LO2 mode of Cu_2O plotted as a function of the *scattered* photon frequency. The solid curves are theoretical curves discussed in text. The broken lines are for guidance of eyes only.

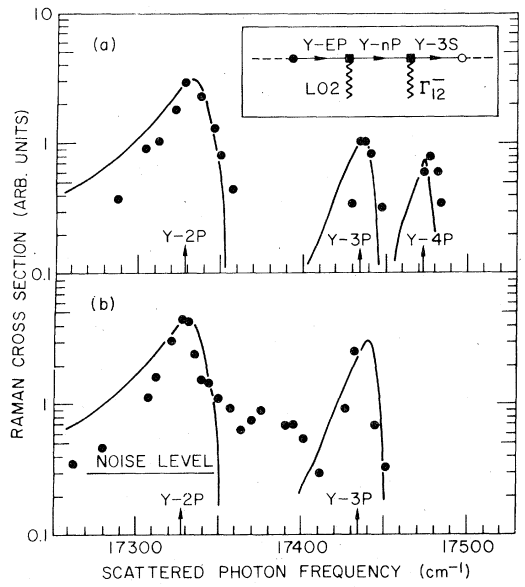

FIG. 7. Raman cross section of the (a) LO1 + Γ_{12}^- and (b) LO2 + Γ_{12}^- mode of Cu_2O plotted as a function of the scattered photon frequency. The solid curves are plots of Eq. (17). The inset shows a diagrammatic representation of a proposed scattering process for the LO2 + Γ_{12}^- mode to explain the extra peak at around 17 380 cm^{-1}. The notations are same as in Fig. 5 except ○ stands for a quadrupole exciton-photon interaction Hamiltonian.

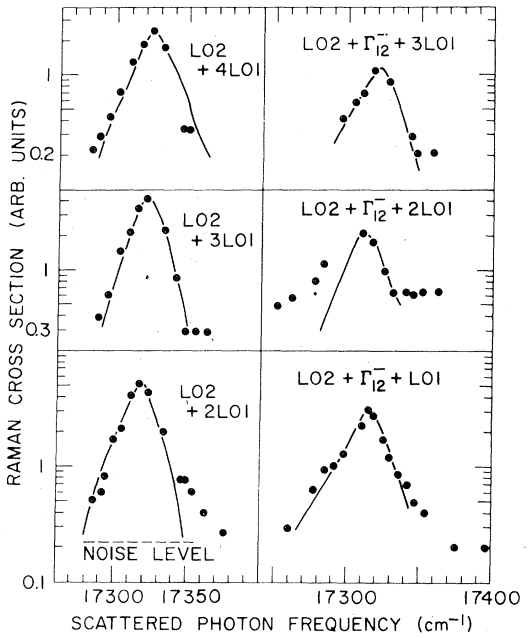

FIG. 8. Raman cross section of multiphonon modes of the form LO2 + (LO1 or Γ_{12}^-) + nLO1 (n = 1, 2, and 3) in Cu_2O plotted on the same vertical scale as a function of the scattered photon frequency. The solid curves are theoretical curves discussed in the text.

hanced. The dependence of its Raman cross section on ν_l is shown in Fig. 5. As ν_l is increased into the yellow exciton continuum, other two phonon modes, Γ_{12}^- + LO1, 2LO1, and LO1 + LO2, appear also. These modes are enhanced due to resonance of the scattered photon frequency ν_s with the Y-nP series, as can be seen from Figs. 6 and 7.

B. Incident photon resonant with the green exciton and scattered photon resonant with the yellow exciton (interexciton scattering)

As ν_l approaches the green excitonic series a large number of high-frequency peaks appeared. These can be grouped into two series of the form LO2 + (LO1 or Γ_{12}^-) + nLO1 (n = 1, 2, and 3) except for a weak LO2 + 2Γ_{12}^- mode. Although the incident photon is now resonant with the green exciton, the enhancement peaks in the Raman cross section of these modes are again better explained by resonances of ν_s with the yellow excitonic series. This is obvious from Fig. 8 where the enhancements of their Raman cross sections when ν_s is in the vicinity of Y-2P are shown.

The width of the multiphonon modes observed in this region was found to increase with the number of phonons scattered. Table I lists their full widths at half-maximum. Comparing these widths with those of the luminescence peaks in Fig. 4(b), it is clear that these multiphonon modes are sharper than the Y-2P peak but comparable in width to the Y-3P and Y-4P peaks. As a result, it is difficult to separate these Raman modes from the luminescence peaks when they overlap, hence the enhancement of these modes at Y-3P and Y-4P could not be determined. Instead we measured the excitation spectra (ES) of the Y-3P and Y-4P peaks. The resultant ES (Figs. 9 and 10) show series of sharp peaks separated from the Y-3P and Y-4P exciton peaks by well-defined phonon frequencies which are indicated in the figures. The fact that these phonon frequencies again fall into

TABLE I. Full widths at half-maximum of multiphonon modes in Cu_2O (at ~2 °K). These widths have not been deconvoluted with a spectrometer slit width of ~3 cm^{-1}.

Mode	Width (cm^{-1})
LO2 + 2LO1	8
LO2 + Γ_{12}^- + LO1	8
LO2 + 2Γ_{12}^-	6
LO2 + 3LO1	10
LO2 + Γ_{12}^- + 2LO1	11
LO2 + 4LO1	12

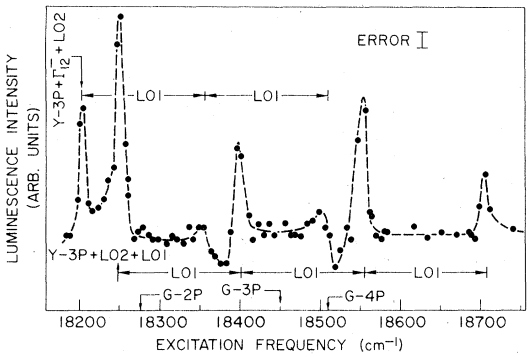

FIG. 9. Excitation spectrum of the Y-3P luminescence peak. Excitation frequencies which exceed the Y-3P luminescence peak by phonon frequencies of the form LO2+(LO1 or Γ_{12}^-)+nLO1 (where n is an integer) are marked. The green exciton discrete levels are indicated by arrows to show that the observed peaks are not related to the green excitons.

two series of the form LO2+(LO1 or Γ_{12}^-)+nLO1 is evidence that these multiphonon modes also resonate with the Y-3P and Y-4P excitons.

C. Both incident and scattered photons resonant with green excitons (intra-green-exciton scattering)

When ν_l is resonant with high energy levels of the green exciton, the 2LO1 mode becomes enhanced again. By plotting its Raman cross section against ν_s the enhancement is found to peak at the G-2P exciton level (see Fig. 11). We have scanned ν_l out to 19 000 cm^{-1} but did not find any more resonances of the 2LO1 mode or of any other Raman modes.

IV. DISCUSSION

In Sec. III we have separated our resonant Raman results in Cu_2O into three separate groups according to their resonant intermediate states. We shall now analyze and discuss them separately.

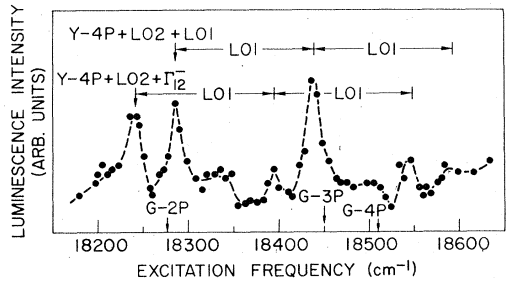

FIG. 10. Excitation spectrum of the Y-4P luminescence peak.

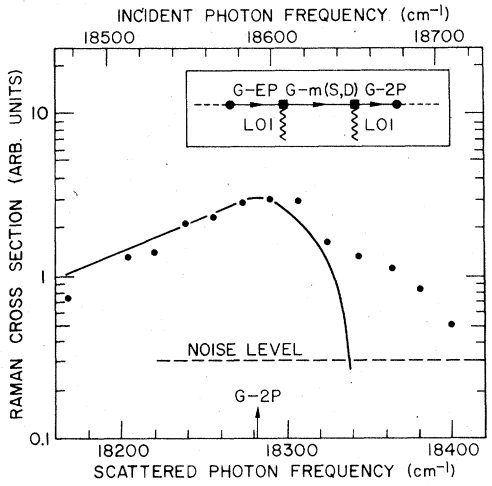

FIG. 11. Raman cross section of the 2LO1 mode plotted as a function of the scattered photon frequency in the vicinity of the green exciton 2P level. The solid curve is a plot of Eq. (22). The inset shows diagrammatically the scattering process responsible for the resonance. The notations are same as in Fig. 5.

A. Intra-yellow-exciton scattering

1. RRS of Γ_{12}^- + LO2 mode

We pointed out in I that there are three types of two-phonon Raman processes but only one type was found to be important in Cu_2O. In this kind of two-phonon scattering process an incident photon excites an exciton which is scattered by two phonons successively before recombining to emit the scattered photon. The dominant contribution to the Raman cross section in such process is given by [Eq. (5) in I]

$$\sigma(\omega_l) \propto \left| \sum_{\alpha,\beta,\gamma} \frac{\langle f|H_{ER}(\omega_s)|\gamma\rangle\langle\gamma|H_{EL}(2)|\beta\rangle}{\omega_\gamma + \omega_0(1) + \omega_0(2) - \omega_l} \times \frac{\langle\beta|H_{EL}(1)|\alpha\rangle\langle\alpha|H_{ER}(\omega_l)|i\rangle}{[\omega_\beta + \omega_0(1) - \omega_l](\omega_\alpha - \omega_l)} \right|^2 . \quad (3)$$

In Eq. (3) $|i\rangle$ and $|f\rangle$ are, respectively, the initial and final states of the solid; $|\alpha\rangle$, $|\beta\rangle$, and $|\gamma\rangle$ are intermediate states with energies $\hbar\omega_\alpha$, $\hbar\omega_\beta$, and $\hbar\omega_\gamma$ respectively; H_{ER} and H_{EL} are exciton-radiation and exciton-phonon Hamiltonians and $\hbar\omega_0(1)$ and $\hbar\omega_0(2)$ are the energies of the two phonons scattered. Summations over α, β, and γ are usually limited to only those intermediate states which minimize the energy denominator in Eq. (3).

We now utilize Eq. (3) to calculate the cross section of the Γ_{12}^-+LO2 mode. The scattering process responsible for the enhancement of this mode is

shown in the inset of Fig. 5. We arrived at this scattering process based on the observation that first the incident photon is resonant with the Y-nP states, and second the Γ_{12}^- phonon is known to be most efficient in assisting radiative recombination of the Y-$1S$ exciton.[7] From Eq. (3) the scattering cross section for the $\Gamma_{12}^-(\vec{q}) + \mathrm{LO2}(-\vec{q})$ phonons is given by

$$\sigma_{\Gamma_{12}^-(\vec{q})+\mathrm{LO2}(-\vec{q})}(\omega_l,\omega_s) \propto \left| \sum_{n,b} \langle 0;\Gamma_{12}^- + \mathrm{LO2};\eta_l - 1;\eta_s + 1 \,|H_{ER}(\omega_s)|\, b;\Gamma_{12}^- + \mathrm{LO2};\eta_l - 1;\eta_s\rangle \right.$$
$$\times \frac{\langle b;\Gamma_{12}^- + \mathrm{LO2};\eta_l - 1;\eta_s \,|H_{EL}(\Gamma_{12}^-)|\, Y\text{-}1S(\vec{q});\mathrm{LO2};\eta_l - 1;\eta_s\rangle}{\omega_s - \omega_b}$$
$$\times \frac{\langle Y\text{-}1S(\vec{q});\mathrm{LO2};\eta_l - 1;\eta_s \,|H_{EL}(\mathrm{LO2})|\, Y\text{-}nP;0;\eta_l - 1;\eta_s\rangle}{\omega_l - \omega_{Y1}(\vec{q}) - \omega_{\mathrm{LO2}} - i\Gamma_{Y1}(\vec{q})}$$
$$\left. \times \frac{\langle Y\text{-}nP;0;\eta_l - 1;\eta_s \,|H_{ER}(\omega_l)|\, 0;0;\eta_l;\eta_s\rangle}{\omega_l - \omega_{Yn} - i\Gamma_{Yn}} \right|^2 . \tag{4}$$

The notations are same as in I. Within each "ket" the first two symbols denote, respectively, the exciton and phonon excited while the last two are the numbers of incident (η_l) and scattered (η_s) photons and b denotes a dipole-allowed exciton. The total cross section of the $\Gamma_{12}^- + \mathrm{LO2}$ mode is then obtained by summing $\sigma_{\Gamma_{12}^-(\vec{q})+\mathrm{LO2}(-\vec{q})}$ over the phonon wave vector $\vec{q}$. We should point out that the exciton-LO-phonon Hamiltonian, $H_{EL}(\mathrm{LO2})$, consists of 2 terms: the usual deformation potential interaction and a Fröhlich interaction due to the macroscopic electric field associated with the phonon.[13] So far, RRS results in various ionic or partially ionic crystals have suggested that at resonance the Fröhlich interaction usually dominates over the deformation potential interaction.[14]

Equation (4) can be simplified if we recall from I that (i) the Γ_{12}^- phonon has no dispersion; (ii) the expression

$$\left| \sum_b \frac{\langle 0;\Gamma_{12}^- + \mathrm{LO2};\eta_l - 1;\eta_s + 1 \,|H_{ER}(\omega_s)|\, b;\Gamma_{12}^- + \mathrm{LO2};\eta_l - 1;\eta_s\rangle}{\omega_s - \omega_b} \right.$$
$$\left. \times \langle b;\Gamma_{12}^- + \mathrm{LO2};\eta_l - 1;\eta_s \,|H_{EL}(\Gamma_{12}^-)|\, Y\text{-}1S;\mathrm{LO2};\eta_l - 1;\eta_s\rangle \right|^2$$

can be taken as a constant; and (iii)

$$\left| \frac{1}{\omega_l - \omega_{Y1}(\vec{q}) - \omega_{\mathrm{LO2}} - i\Gamma_{Y1}(\vec{q})} \right|^2 \simeq \frac{\pi\delta(\omega_l - \omega_{Y1}(\vec{q}) - \omega_{\mathrm{LO2}})}{\gamma_1(\omega_l - \omega_{Y1} - \omega_{\mathrm{LO2}})} , \tag{5}$$

where

$$\Gamma_{Y1} \equiv \gamma_1(x) = A + x + B(x - 2\omega_{12})^{1/2} \quad \text{for } x > 2\omega_{12} , \tag{6}$$

$\hbar\omega_{12}$ being the energy of the Γ_{12}^- phonon; A and B are constants introduced in Eq. (27) of I; and

$$\omega_{Y1}(\vec{q}) = \omega_{Y1} + \hbar q^2/2M, \tag{7}$$

M being the effective mass of the Y-$1S$ exciton.

Utilizing these results, the total cross section of the $\Gamma_{12}^- + \mathrm{LO2}$ mode can be written

$$\sigma_{\Gamma_{12}^- + \mathrm{LO2}}(\omega_l) \propto (\omega_l - \omega_{Y1} - \omega_{\mathrm{LO2}})^{1/2}\gamma_1^{-1}$$
$$\times \left| \sum_n \frac{\langle Y\text{-}1S(q_2);\mathrm{LO2};\eta_l - 1;\eta_s \,|H_{EL}(\mathrm{LO2})|\, Y\text{-}nP;0;\eta_l - 1;\eta_s\rangle}{\omega_l - \omega_{Yn} - i\Gamma_{Yn}} \right.$$
$$\left. \times \langle Y - nP;0;\eta_l - 1;\eta_s \,|H_{ER}(\omega_l)|\, 0;0;\eta_l;\eta_s\rangle \right|^2 . \tag{8}$$

In Eq. (8) we have introduced a wave vector $\vec{q}_2$ defined by $\omega_{Yn} = \omega_{Y1}(\vec{q}_2) + \omega_{\mathrm{LO2}}$. As it stands, Eq. (8) can be calculated exactly since all the parameters involved are either known from other experiments or can be calculated.

In particular, the Fröhlich matrix elements

$$F_{1S,nP}^{(2)}(q) = \langle Y\text{-}1S(q);\mathrm{LO2};\eta_l - 1;\eta_s \,|H_{EL}(\mathrm{LO2})|\, Y\text{-}nP;0;\eta_l - 1;\eta_s\rangle$$

TABLE II. Fröhlich matrix elements $F^{(1)}_{nP,1S}(k_1)$ and $F^{(2)}_{nP,1S}(k_2)$ in units of iAa_0, with wave vectors k_i defined by $\omega_{Yn}-\omega_{Y1}-\omega_{LOi}=\hbar k_i^2/2M (i=1,2)$.

n	$F^{(1)}_{nP,1S}(k_1)=\langle nP\vert H_{EL}(\mathrm{LO1})\vert 1S(k_1)\rangle$	$F^{(2)}_{nP,1S}(k_2)=\langle nP\vert H_{EL}(\mathrm{LO2})\vert 1S(k_2)\rangle$
2	0.177	0.476
3	0.089	0.202
4	0.056	0.122
5	0.040	0.085

have been calculated in the Appendix (see Table II), assuming a hydrogenic model for the yellow exciton. However, to facilitate comparison with experiment, we made further simplifications in Eq. (8). The linewidths of the lower-energy yellow-exciton levels ($n=2,3,4$, and 5) are small enough so that their contributions to the summation in Eq. (8) do not interfere. As a result we can make use of the relationship

$$\alpha_{Yn}(\omega_l)\propto\left|\langle Y\text{-}nP;0;\eta_l-1;\eta_s\left|H_{ER}(\omega_l)\right|0;0;\eta_l;\eta_s\rangle\right|^2(\Gamma_{Yn}/\pi)[(\omega_l-\omega_{Yn})^2+\Gamma_{Yn}^2]^{-1}$$

and express $\sigma_{\Gamma_{12}^-+\mathrm{LO2}}(\omega_l)$ as

$$\sigma_{\Gamma_{12}^-+\mathrm{LO2}}(\omega_l)\propto\sum_n\alpha_{Yn}(\omega_l)\left|F^{(2)}_{1S,nP}(q_2)\right|^2(\omega_l-\omega_{Y1}-\omega_{\mathrm{LO}2})^{1/2}\gamma_1^{-1}\Gamma_{Yn}^{-1},\tag{9}$$

where $\alpha_{Yn}(\omega_l)$ is the absorption constant due to the Y-nP exciton. The meaning of Eq. (9) is simply that the RRS of the $\Gamma_{12}^-+\mathrm{LO2}$ mode can be treated as a three-step absorption-emission process: absorption of incident photon in exciting the Y-nP exciton (probability proportional to α_{Yn}); scattering of the Y-nP exciton to the Y-$1S$ state by the LO2 phonon [probability proportional to $\left|F^{(2)}_{1S,nP}(q_2)\right|^2\Gamma_{Yn}^{-1}$], and Γ_{12}^- phonon-assisted radiative recombination of the Y-$1S$ exciton [probability proportional to $(\omega_l-\omega_{Y1}-\omega_{\mathrm{LO}2})^{1/2}\gamma_1^{-1}$ calculated in I].

The advantage of using Eq. (9) to calculate $\sigma_{\Gamma_{12}^-+\mathrm{LO2}}$ is that the renormalization of the exciton-radiation Hamiltonian $H_{ER}(\omega_l)$ and the exciton energies $\hbar\omega_{Yn}$ due to exciton-photon interaction[15] is automatically included in the absorption constant $\alpha_{Yn}(\omega_l)$ which can be obtained experimentally. The solid curves in Fig. 5 have been calculated from Eq. (9) with only one adjustable parameter; namely, the experimental and theoretical results are normalized at $\omega_l=\omega_{Y3}$. In general, the agreement between experiment and theory is good. Most of the discrepancies can probably be explained by uncertainty in deducing $\alpha_{Yn}(\omega_l)$ from the experimental absorption curve in Fig. 4(a) due to the phonon-assisted absorption background and by the fact that for $n\gtrsim 5$ the discrete levels of the yellow exciton begin to overlap so that the cross terms in Eq. (9) are no longer negligible.

It is usually assumed that both the LO1 and LO2 phonons can be responsible for the relaxation of the Y-nP ($n\geq 2$) excitons in Cu_2O. Thus one would expect the $\Gamma_{12}^-+\mathrm{LO1}$ mode to show resonance enhancements similar to the $\Gamma_{12}^-+\mathrm{LO2}$ mode. We found, however, that $\sigma_{\Gamma_{12}^-+\mathrm{LO1}}$ is smaller than $\sigma_{\Gamma_{12}^-+\mathrm{LO2}}$ by typically one order of magnitude mainly because $|F^{(2)}_{1S,nP}(q_2)|^2\gg|F^{(1)}_{1S,nP}(q_1)|^2$ (see Table II) where $F^{(1)}_{1S,nP}$ stands for the Fröhlich matrix element of LO1 and $\tilde{q}_1$ is defined by $\omega_{Yn}=\omega_{Y1}(\tilde{q}_1)+\omega_{\mathrm{LO}1}$. This is due to the fact that the energy separation of the Y-nP states from the Y-$1S$ level is much closer to the energy of the LO2 phonon so that the "spanning" wave vector q_1 for LO1 is much larger than q_2 for LO2. The Fröhlich matrix elements fall off rapidly at large wave vectors.[16]

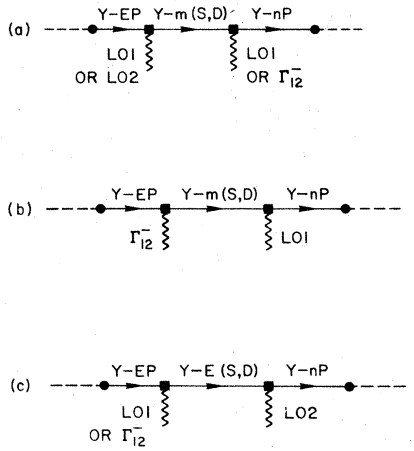

FIG. 12. Diagrammatic representations of the scattering processes responsible for the resonant enhancements of the 2LO1, $\mathrm{LO}_1+\Gamma_{12}^-$, LO2+LO1, and LO2 $+\Gamma_{12}^-$ modes shown in Figs. 6 and 7.

2. RRS of two-phonon modes: (LO1 or LO2) + (LO1 or Γ_{12}^-)

Resonance enhancement of the LO2 + Γ_{12}^- mode also occurs when the incident photon is resonant with the yellow exciton continuum while the scattered photon is resonant with the discrete Y-nP levels. This in fact occurs for all the two-phonon modes of the form (LO1 or LO2) + (LO1 or Γ_{12}^-) as shown in Figs. 6 and 7. The Raman processes which contribute to the observed resonances are shown diagrammatically in Fig. 12.

We first analyze the 2LO1 mode in detail because in this case only process (a) in Fig. 12 has to be considered. The scattering cross section, using Eq. (3), is given by

$$\sigma_{2\mathrm{LO1}}(\omega_l;\omega_s)\propto\sum_{\vec{q},E}\left|\sum_{n,m}\sum_{X=S,D,F\ldots}\frac{\langle 0;2\mathrm{LO1};\eta_l-1;\eta_{s+1}|H_{ER}(\omega_s)|Y\text{-}nP;2\mathrm{LO1};\eta_l-1;\eta_s\rangle}{\omega_s-\omega_{Yn}-i\Gamma_{Yn}}\right.$$
$$\left.\times\frac{F^{(1)}_{nP,mX}(q)\,F^{(1)}_{mX,EP}(q)\langle Y\text{-}EP;0;\eta_l-1;\eta_s|H_{ER}(\omega_l)|0;0;\eta_l;\eta_s\rangle}{[\omega_l-\omega_{\mathrm{LO1}}-\omega_{Ym}(\vec{q})-i\Gamma_{Ym}(\vec{q})](\omega_l-E/\hbar-i\Gamma_c)}\right|^2. \quad (10)$$

$F^{(1)}_{mX,EP}$ stands for the Fröhlich matrix element between the discrete level mX and the continuum P state (with energy E) of the yellow exciton. These Fröhlich matrix elements as a function of q have not been evaluated and so we shall neglect their wave vector dependence. Their $q=0$ values have been calculated by several authors.[17] In the Appendix we have listed in Table V $F^{(1)}_{mS,EP}(q\sim 0)$ and $F^{(1)}_{mD,EP}(q\sim 0)$ for two values of E corresponding to $\omega_s = E/\hbar - 2\omega_{\mathrm{LO1}} \simeq \omega_{Y2}$ and ω_{Y3} respectively.

To simplify Eq. (10) we shall make the following approximations: (i) summation over X is limited to the S and D states; (ii) summation over n is limited to one single value such that $\omega_s \sim \omega_{Yn}$; and (iii) interference between contributions from the different mX intermediate states will be neglected; i.e., $|\sum_m \cdots|^2$ will be replaced by $\sum_m |\cdots|^2$.

With these approximations we can then express Eq. (10) as the cross section of a multistep absorption-emission process,

$$\sigma_{2\mathrm{LO1}}(\omega_l;\omega_s\sim\omega_{Yn})\propto\alpha_{YE}(\hbar\omega_l)\left(\sum_{q,m}|F^{(1)}_{nP,mS}(q)\,F^{(1)}_{mS,EP}+F^{(1)}_{nP,mD}(q)\,F^{(1)}_{mD,EP}|^2\right.$$
$$\left.\times\delta(\omega_l-\omega_{\mathrm{LO1}}-\omega_{Ym}(q))/\Gamma_{YE}\Gamma_{Ym}\right)\frac{\alpha_{Yn}(\omega_S)}{\Gamma_{Yn}}, \quad (11)$$

where $\alpha_{YE}(\omega_l)$, the absorption coefficient at incident photon frequency ω_l, gives the probability of exciting the yellow-exciton continuum;

$$\sum_{q,m}|F^{(1)}_{nP,mS}(q)\,F^{(1)}_{mS,EP}+F^{(1)}_{nP,mD}(q)\,F^{(1)}_{mD,EP}|^2/\Gamma_{YE}\Gamma_{Ym}$$

is the probability of successive exciton scattering from Y-EP to Y-(mS, mD) and then to Y-nP by two LO1 phonons, and $\alpha_{Yn}(\omega_s)/\Gamma_{Yn}$ is the probability of emitting a photon at ω_s from recombination of the Y-nP exciton. In general, for a given n we find that a few Fröhlich matrix elements are much larger than the rest and typically it is sufficient to sum m from $n-2$ to $n+2$. As an example, we consider the $n=2$ case. From Tables III–V the largest matrix elements are $|F^{(1)}_{2P,2S}(q_1)F^{(1)}_{2S,EP}|^2$ and $|F^{(1)}_{2P,3D}(q_1)F^{(1)}_{3D,EP}|^2$. They are stronger than the other matrix elements by at least a factor of 4. However, due to the uncertainty in the position and oscillator strength of the 2S state, we shall take

TABLE III. Matrix elements $F^{(1)}_{mS,nP}(k)=\langle mS|H_{EL}(\mathrm{LO1})|nP(k)\rangle$ (in units of iAa_0) for LO1 phonon wave vector $k=0$ and $k=q_1$ where q_1 is defined by $|\omega_{Yn}-\omega_{Ym}|-\omega_{\mathrm{LO1}}=\hbar q_1^2/2(m_e+m_h)$.

m \ n	2		3		4		5	
	$k=0$	$k=q_1$	$k=0$	$k=q_1$	$k=0$	$k=q_1$	$k=0$	$k=q_1$
1	0.75	0.177	0.297	0.089	0.175	0.056	0.12	0.4
2	−3.0	−1.15	1.77	−0.209	0.74	−0.102	0.45	−0.064
3	0.545	−0.078	−7.34	−0.0007	3.16	−0.01	1.30	−0.0097
4	0.22	−0.109	1.41	−0.198	−13.4	−0.085	4.92	−0.048
5	0.132	−0.083	0.56	−0.293	2.66	−0.065	−21.21	−0.027
6	0.91	−0.065	0.33	−0.222	1.03	−0.041	4.28	−0.0135
7	0.069	−0.052	0.23	−0.188	0.60	−0.027	1.67	−0.011
8	0.054	−0.042	0.17	−0.158	0.41	−0.021	0.95	−0.011

TABLE IV. Fröhlich matrix elements $F^{(1)}_{mD,nP}(k) = \langle mD|H_{EL}(\mathrm{LO1})|nP(k)\rangle$ (in units of iAa_0) for LO1 phonon wave vector $k=0$ and $k=q_1$.

m \ n	2		3		4		5	
	$k=0$	$k=q_1$	$k=0$	$k=q_1$	$k=0$	$k=q_1$	$k=0$	$k=q_1$
3	6.7	4.32	−14.2	0.159	1.837	0.0545	0.681	0.030
4	2.41	1.72	10.67	−0.331	−29.32	−0.11	4.29	−0.053
5	1.38	1.04	4.188	−0.22	15.57	−0.143	−48.5	0.01
6	0.93	0.724	2.46	−0.073	6.189	0.03	21.39	0.022
7	0.694	0.548	1.69	0.012	3.65	0.037	8.47	0.013
8	0.544	0.435	1.27	0.056	2.52	0.033	4.98	0.004

only the $3D$ level as the resonant intermediate state. This allows us to write the Raman cross section of the 2LO1 mode as

$$\sigma_{2\mathrm{LO1}}(\omega_l;\omega_s\sim\omega_{Y2}) \propto \frac{\alpha_{YE}(\hbar\omega_l)\alpha_{Y2}(\hbar\omega_s)}{\Gamma_{YE}\Gamma_{Y2}\Gamma_{Y3}}\,|F^{(1)}_{2P,3D}(q_1)F^{(1)}_{3D,EP}|^2 \times\begin{cases}(\omega_s+\omega_{\mathrm{LO1}}-\omega_{Y3})^{1/2} & \text{if } \omega_s+\omega_{\mathrm{LO1}}\geq\omega_{Y3}\\ 0 & \text{otherwise.}\end{cases} \tag{12}$$

Equation (12) is plotted in Fig. 6(a) as the solid curve peaked at Y-$2P$. Except for an overall normalization constant the agreement between theory and experiment is quite good.

In case of the resonances at Y-$3P$ and Y-$4P$ we do not find a single dominant Fröhlich matrix element. For the Y-$3P$ resonance we have used the Fröhlich matrix elements in Tables III–V to evaluate explicitly the quantity

$$M_{2\mathrm{LO1}}(n,\omega_s)=\sum_q\sum_{m=2}^{6}|F^{(1)}_{nP,mS}(q)F^{(1)}_{mS,EP} + F^{(1)}_{nP,mD}(q)F^{(1)}_{mD,EP}|^2 \times\delta(\omega_l+\omega_{\mathrm{LO1}}-\omega_{Ym}(q))\,\Gamma_{Ym}^{-1} \quad \text{with } n=3, \tag{13}$$

TABLE V. Fröhlich matrix elements $F^{(1)}_{mS,EP}$ and $F^{(1)}_{mD,EP}$ [in units of $iAa_0/(2\pi)^{3/2}$] of E ($E/2\pi\hbar c = 17\,592$ and $17\,720\ \mathrm{cm}^{-1}$) corresponding to $\epsilon'=0.085$ and 0.25 Ry, respectively.

m	$\epsilon'=0.085$ Ry		$\epsilon'=0.25$ Ry	
	$F^{(1)}_{mS,EP}$	$F^{(1)}_{mD,EP}$	$F^{(1)}_{mS,EP}$	$F^{(1)}_{mD,EP}$
2	6.12		11.9	
3	−25.4	−3.41	−10.73	−0.828
4	4.88	4.96	9.04	0.88
5	1.94	−5.44	···	−0.795
6	1.14	5.39	···	0.687
7	0.80	−5.05	···	···
8	0.59	4.62	···	···

but found it to be almost independent of ω_S in the vicinity of ω_{Y3}. Since $\alpha_{YE}(\omega_l)$ is a slowly varying function of ω_l we can simplify Eq. (11) to

$$\sigma_{2\mathrm{LO1}}(\omega_S\sim\omega_{Yn})\propto\alpha_n(\omega_S)\quad(n=3,4). \tag{14}$$

Equation (14) is plotted as solid curves in Fig. 6(a) by normalizing the theoretical and experimental curves at the peak of each resonance. The agreement between theory and experiment is not as good as the $\omega_S\sim\omega_{Y2}$ resonance. Typically, the experimental peaks are much sharper than the theoretical curves. The reason for this discrepancy probably lies in the term $M_{2\mathrm{LO1}}$. Although we do not find strong dispersion in $M_{2\mathrm{LO1}}$, there are interferences between terms arising from different mS and mD intermediate states. These interferences are very sensitive to the accuracy of the Fröhlich matrix elements. Thus the narrow width of the resonance peaks at $\omega_S\sim\omega_{Y3}$ and ω_{Y4} can probably be explained by calculating the Fröhlich matrix elements with a more realistic model than the hydrogenic model for the yellow exciton.

Resonances in the LO1 + LO2 mode may arise from scattering processes (a) or (c) shown in Fig. 12. The similarity in the shape of the $\omega_S\sim\omega_{Y2}$ resonance peaks for the 2LO1 and LO1 + LO2 mode suggests that process (a) is probably more important. Under such assumption we can obtain the LO2 + LO1 mode Raman cross section in the same way as $\sigma_{2\mathrm{LO1}}$,

$$\sigma_{\mathrm{LO2+LO1}}(\omega_l;\omega_s\sim\omega_{Y2}) \propto \frac{\alpha_{YE}(\hbar\omega_l)\alpha_{Y2}(\hbar\omega_s)}{\Gamma_{YE}\Gamma_{Y2}\Gamma_{Y3}}\,|F^{(1)}_{2P,3D}(q_1)|^2|F^{(2)}_{3D,EP}|^2 \times\begin{cases}(\omega_s+\omega_{\mathrm{LO1}}-\omega_{Y3})^{1/2} & \text{if } \omega_s\geq\omega_{Y3}-\omega_{\mathrm{LO1}}\\ 0 & \text{otherwise.}\end{cases} \tag{15}$$

Thus the functional dependence of $\sigma_{\mathrm{LO2+LO1}}$ on ω_S is identical to that of $\sigma_{2\mathrm{LO}}$ ($\omega_S\sim\omega_{Y2}$). It is shown as the solid line in Fig. 6(b). The good agreement between theory and experiment thus supports our assumption that process (a) in Fig. 12 is more important than process (c).

We did not attempt to explain quantitatively the $\omega_S \sim \omega_{Y3}$ resonance of the LO2 + LO1 mode in Fig. 6(b) due to lack of reliable Fröhlich matrix elements. We note that in this case the enhancement peak in the Raman cross section is again sharper than the corresponding absorption peak.

We next consider the LO1 + Γ_{12}^- and LO2 + Γ_{12}^- modes in Fig. 7. Their Raman cross sections can again be calculated from the diagrams in Fig. 12,

$$\sigma_{\mathrm{LO}x+\Gamma_{12}^-}(\omega_l;\omega_S \sim \omega_{Yn}) \propto \alpha_{YE}(\hbar\omega_l)\alpha_{Yn}(\hbar\omega_S) \times M_{\mathrm{LO}x+\Gamma_{12}^-}\Gamma_{YE}^{-1}\Gamma_{Yn}^{-1} \quad (x=1,2;\ n=2,3,4), \tag{16}$$

where $M_{\mathrm{LO}x+\Gamma_{12}^-}$ $(x=1,2)$ is defined in a way analogous to $M_{2\mathrm{LO1}}$ in Eq. (13). Again for simplicity we assume that $M_{\mathrm{LO}x+\Gamma_{12}^-}$ $(x=1,2)$ has no dispersion and $\alpha_{YE}(\hbar\omega_l)$ is slowly varying so Eq. (16) is simplified to

$$\sigma_{\mathrm{LO}x+\Gamma_{12}^-}(\omega_S \sim \omega_{Yn}) \propto \alpha_{Yn}(\hbar\omega_S) \quad (x=1,2;n=2,3,4). \tag{17}$$

Equation (17) is plotted in Fig. 7 as solid curves, each normalized to the experimental peaks. The agreement between theory and experiment is not quite satisfactory. In all cases the experimental curves are narrower than the theoretical curves. Again this discrepancy could be caused by interference in the intermediate states which was neglected in assuming $M_{\mathrm{LO}x+\Gamma_{12}^-}$ $(x=1,2)$ to be constant. In case of the LO2 + Γ_{12}^- mode in Fig. 7(b) we note that there is a small peak lying between the Y-2P and Y-3P levels which is absent in the theory. Since the frequency of this peak (~17 380 cm^{-1}) coincides with that of the Y-3S exciton level we propose that this peak is due to resonance of ω_S with the Y-3S level. The scattering process which could produce this resonance is shown diagrammatically in the inset of Fig. 7. The width of this extra peak in Fig. 7(b) is also consistent with the Γ_{12}^- phonon resonance at Y-3S.[3] More quantitative test of this explanation is not possible since very little information is available on the Y-3S level.

B. Scattering between the green and yellow excitons

1. *RRS of multiphonon modes at Y-2P exciton*

A large number of Raman modes involving more than two phonons appear when the incident and scattered photons are resonant with the green and yellow excitons, respectively. These multiphonon modes can be divided into two series of the form LO2 + (LO1 or Γ_{12}^-) + nLO1, where n = 1, 2, and 3. Furthermore, these modes have the following properties:

(i) The resonance peaks in the Raman cross sections occur when the *scattered* photon is resonant with the Y-2P exciton level (see Fig. 8).

(ii) Although we have observed Raman scattering of the LO2 phonon plus as many as four LO1 phonons, scattering of LO1 phonons alone has been observed only up to two LO1 phonons.

(iii) Raman scattering of odd-parity phonon modes is normally forbidden in a centrosymmetric crystal like Cu_2O. Odd-parity modes have been observed in Cu_2O only when either the incident or the scattered photon is resonant with excitons of S and D symmetries.[1-3] In these cases, the photon at resonance induces an electric quadrupole or magnetic dipole transition.[2,18] In the present case, however odd-parity Raman modes (e.g., LO2 + 2LO1 and LO2 + LO1 + Γ_{12}^-) are observed at resonance with P states of the yellow exciton.

(iv) Cross sections of the LO2 + (LO1 or Γ_{12}^-) + nLO1 Raman modes decrease very slowly with increase in n for $n \leq 3$ (vertical scales for all curves in Fig. 8 are the same). Then the cross section for the n = 4 mode drops by almost an order of magnitude from n = 3 (the LO2 + 5LO1 mode was observable with a signal-to-noise ratio of only about 2).

To explain these observations, we propose the following model for the scattering of these multiphonon modes. The incident photon excites a green exciton which decays by emission of up to two LO1 phonons down to the G-2P level. The G-2P exciton scatters into the continuum of the yellow exciton by emission of one LO2 phonon. The yellow exciton then relaxes from the continuum to the discrete nP levels by emitting either two LO1 phonons or one LO1 phonon plus a Γ_{12}^- phonon as discussed in Sec. IV A.

This model is essentially the same as the cascade model proposed by Martin and Varma.[19] The cascade processes involved here for the different multiphonon modes can be schematically represented as

LO2 + LO1 + (LO1, Γ_{12}^-): $G \overset{\mathrm{LO2}}{\rightarrow} Y \overset{\mathrm{LO1}}{\rightarrow} Y^{\mathrm{LO1}}$ or $\Gamma_{12}^- Y$,

LO2 + 2LO1 + (LO1, Γ_{12}^-):

$$G \overset{\mathrm{LO1}}{\rightarrow} G \overset{\mathrm{LO2}}{\rightarrow} Y \overset{\mathrm{LO1}}{\rightarrow} Y^{\mathrm{LO1}} \text{ or } \Gamma_{12}^- Y,$$

LO2 + 3LO1 + (LO1, Γ_{12}^-):

$$G \overset{\mathrm{LO1}}{\rightarrow} G \overset{\mathrm{LO1}}{\rightarrow} G \overset{\mathrm{LO2}}{\rightarrow} Y \overset{\mathrm{LO1}}{\rightarrow} Y \overset{\mathrm{LO1}}{\rightarrow} Y^{\mathrm{LO1}} \text{ or } \Gamma_{12}^- Y,$$

where G and Y stands for a green- and yellow-exciton state, respectively.

From the above processes it is clear why the modes have the form LO2 + (LO1, Γ_{12}^-) + nLO1 (n = 1, 2, and 3). Intra-yellow- and intra-green-exciton scatterings involving more than two phonons have very small probabilities based on the RRS results in the rest of this paper. It is also rea-

sonable to assume that the LO2 phonon is responsible for relaxation of the G-$2P$ exciton to the yellow exciton since one LO2 phonon carries several times more energy than the other odd-parity phonons of Cu_2O. The strength of the odd-parity Raman modes can be explained by intraband scattering of the LO1 phonons via the Fröhlich interaction.[20]

It is difficult to make the above cascade model quantitative since there is a large number of possible intermediate states involving unknown electron-phonon matrix elements. We will assume instead, in a heuristic manner, that the Raman cross section for these multiphonon modes in the cascade process can be written as

$$\left\{\begin{matrix}\sigma_{\mathrm{LO2+LO1}+n\mathrm{LO1}}(\omega_l;\omega_s\sim\omega_{Y2})\\ \sigma_{\mathrm{LO2}+\Gamma_{12}^-+n\mathrm{LO1}}(\omega_l;\omega_s\sim\omega_{Y2})\end{matrix}\right\}$$
$$\simeq\frac{\alpha_G(\omega_l)(P_{G\to G})^{n-1}P_{G\to Y}}{\alpha_Y[\omega_l-\omega_{\mathrm{LO2}}-(n-1)\omega_{\mathrm{LO1}}]}\times\left\{\begin{matrix}\sigma_{2\mathrm{LO1}}(\omega_s\sim\omega_{Y2})\\ \sigma_{\mathrm{LO1}+\Gamma_{12}^-}(\omega_s\sim\omega_{Y2})\end{matrix}\right\},\quad(18)$$

where $P_{G\to G}$ is the probability of intra-green-exciton scattering by a LO1 phonon and $P_{G\to Y}$ is the probability of a G-$2P$ exciton scattering into a yellow exciton by emitting a LO2 phonon. The probability for the remaining steps in the cascade process is taken care of by

$$\alpha_Y[\omega_l-\omega_{LO2}-(n-1)\omega_{\mathrm{LO1}}]^{-1}\left\{\begin{matrix}\sigma_{2\mathrm{LO1}}(\omega_s\sim\omega_{Y2})\\ \sigma_{\mathrm{LO1}+\Gamma_{12}^-}(\omega_s\sim\omega_{Y2})\end{matrix}\right.,$$

taking advantage of the fact that $\sigma_{2\mathrm{LO1}}$ and $\sigma_{\mathrm{LO}+\Gamma_{12}^-}$ can be obtained from the experimental or theoretical curves in Figs. 6(a) and 7(a). In general, $P_{G\to G}$ and $P_{G\to Y}$ are energy dependent. For simplicity, we assume they are constant and similarly for $\alpha_Y[\omega_l-\omega_{\mathrm{LO2}}-(n-1)\omega_{\mathrm{LO1}}]$ which is a slowly varying function of ω_l. Thus, we arrive at a simple phenomenological equation,

$$\left\{\begin{matrix}\sigma_{\mathrm{LO2+LO1}+n\mathrm{LO1}}(\omega_l;\omega_s\sim\omega_{Y2})\\ \sigma_{\mathrm{LO2}+\Gamma_{12}^-+n\mathrm{LO1}}(\omega_l;\omega_s\sim\omega_{Y2})\end{matrix}\right\}$$
$$\propto\alpha_G(\omega_l)\left\{\begin{matrix}\sigma_{2\mathrm{LO1}}(\omega_s\sim\omega_{Y2})\\ \sigma_{\mathrm{LO1}+\Gamma_{12}^-}(\omega_s\sim\omega_{Y2})\end{matrix}\right..\quad(19)$$

The solid curves in Fig. 8 are calculated using Eq. (19) and the experimental spectra of $\sigma_{2\mathrm{LO1}}$, $\sigma_{\mathrm{LO1}+\Gamma_{12}^-}$, and $\alpha_G(\omega_l)$.[9,21] For each curve the theoretical peak height has been normalized to the experiment. In some cases an additional slight displacement (typically $\lesssim 10\ \mathrm{cm}^{-1}$) of the theoretical peak relative to the experimental peak position is necessary (probably caused by the $\sim 10\ \mathrm{cm}^{-1}$ spacing between experimental points). Except for this, Eq. (19) accounts satisfactorily for the experimental results.

2. Luminescence excitation spectra of the Y-3P and Y-4P peaks

Photoluminescence spectrum associated with excited states of the yellow-exciton series in Cu_2O was first reported by Compaan and Cummins using an Ar^+ laser as the source of excitation.[22] It was not observed by us in our earlier work using a Rhodamine 6G dye laser.[8] The reason as we now understand it is that this luminescence in Cu_2O does not appear until the excitation frequency is well into the yellow-exciton continuum. The Y-nP luminescence peaks gradually rise out of the background noise as the excitation frequency is increased above $17\,900\ \mathrm{cm}^{-1}$. In other words, there is no sharp onset in the excitation spectra of these luminescence peaks like that of the Y-$1S$ peak.[11] Although at higher-excitation frequencies sharp peaks are observed in excitation spectra of the Y-$3P$ and Y-$4P$ luminescence shown in Figs. 9 and 10, these can be explained by enhancement of multiphonon modes of the form LO2+(LO1 or Γ_{12}^-) $+n$LO1 ($n=1$, 2, and 3) at the Y-$3P$ and Y-$4P$ exciton levels due to the cascade processes proposed in Sec. IV B 1. In Figs. 9 and 10 we have indicated the frequencies at which these multiphonon modes would appear in the Y-$3P$ and Y-$4P$ excitation spectra and most of the sharp peaks in Figs. 9 and 10 can be explained this way.

C. Intra-green-exciton scattering: RRS of 2LO1 mode at G-2P level

The 2LO1 mode becomes enhanced again as the incident photon is tuned to the green exciton continuum and the scattered photon is resonant with the G-$2P$ level. In analogy to its enhancement with the yellow exciton [Fig. 6(a)] we expect the most important Raman process to be that shown in the inset of Fig. 11 [compare with Fig. 12(a)]. The corresponding expression for $\sigma_{2\mathrm{LO1}}(\omega_l;\omega_s\sim\omega_{G2})$ can be derived in the same way as $\sigma_{2\mathrm{LO1}}(\omega_l;\omega_s\sim\omega_{Y2})$:

$$\sigma_{2\mathrm{LO1}}(\omega_l;\omega_s\sim\omega_{G2})\propto\frac{\alpha_{GE}(\hbar\omega_l)\alpha_{G2}(\hbar\omega_s)}{\Gamma_{GE}\Gamma_{G2}}\sum_{q,m}\left|F'^{(1)}_{2P,mS}(q)F'^{(1)}_{mS,EP}+F'^{(1)}_{2P,mD}(q)F'^{(1)}_{mD,EP}\right|^2\frac{\delta(\omega_l-\omega_{\mathrm{LO1}}-\omega_{Gm}(q))}{\Gamma_{Gm}},\quad(20)$$

where the notations are similar to those of Eq. (11) except that in all subscripts G (for green exciton) has replaced Y and that the Fröhlich matrix elements involving the green-exciton states are denoted by F'.

Again for the sake of simplicity we assume the term

$$M'_{2\mathrm{LO}1}(2,\omega_s)=\sum_{q,m}\left|F'^{(1)}_{2P,mS}(q)F'^{(1)}_{mS,EP}+F'^{(1)}_{2P,mD}(q)F'^{(1)}_{mD,EP}\right|^2\times\delta(\omega_l-\omega_{\mathrm{LO}1}-\omega_{Gm}(q))\Gamma^{-1}_{Gm} \quad (21)$$

to be constant so that Eq. (20) becomes

$$\sigma_{2\mathrm{LO}1}(\omega_l;\omega_s\sim\omega_{G2})\propto\alpha_{GE}(\hbar\omega_l)\alpha_{G2}(\hbar\omega_s)\,. \quad (22)$$

Using the green-exciton absorption curves in Ref. 21 we obtain the solid curve in Fig. 11. Although the agreement between theory and experiment is quite satisfactory for ω_s on the low-energy side of the G-$2P$ exciton peak, there are large discrepancies on the high-energy side. This can be due to two sources: (i) over-subtraction of the background absorption in Ref. 21. Two other possible ways to substract the background absorption have been suggested in Ref. 9. In both cases α_{G2} will decrease less abruptly on the high-energy side so the theoretical fit to the experimental results in Fig. 11 will be improved. (ii) $M'_{2\mathrm{LO}1}$ is expected to show dispersion when $\omega_l-\omega_{\mathrm{LO}1}=\omega_{G3}$ and ω_{G4}. These frequencies correspond roughly to ν_s = 18 296 and 18 356 cm^{-1}. We note that these are the frequencies where the experimental $\sigma_{2\mathrm{LO}1}$ seems to show shoulders.

V. CONCLUSION

Multiphonon resonant Raman scattering has been studied in Cu_2O by tuning a dye laser across its yellow and green excitonic absorption regions. Enhancement of a large number of phonon modes has been observed. Quantitative theories have been proposed to explain the observed resonances in terms of intra- and interexciton scatterings by phonons. In general, satisfactory agreement between theory and experiment was found.

Based on the resonant Raman results the following exciton relaxation mechanisms in Cu_2O have been deduced:

From	To	Phonon(s) emitted
G-nP	G-$2P$	LO1 phonons
G-$2P$	Y-EP	LO2 phonon
Y-EP	Y-nP	Γ^-_{12} or LO1 phonons ($E/\hbar-\omega_{Y\infty}<\omega_{\mathrm{LO}2}$)
		LO2 phonon ($E/\hbar-\omega_{Y\infty}>\omega_{\mathrm{LO}2}$)
Y-nP	Y-$1S$	LO2 phonon
$Y-1S$ $(q\neq0)$	Y-$1S$ $(q\simeq0)$	LA phonons[7]

This scheme of exciton relaxation provides an explanation for the excitation dependence of the yellow exciton luminescence. When the excitation frequency ν_l is in the region of the discrete yellow-exciton levels, the yellow excitons relax rapidly to the Y-$1S$ level by emission of a LO2 phonon. Therefore, in this region only a Raman mode (LO2 + Γ^-_{12}) is observed. When ν_l is resonant with the yellow exciton continuum, but not far above the discrete exciton levels, the photoexcited excitons can relax down to the Y-nP levels by emission of a small number of phonons (LO1 or Γ^-_{12}). Thus the relaxed Y-nP excitons are mostly not thermalized before recombination, resulting in the resonant Raman scattering of the two-phonon modes shown in Figs. 6(a) and 7(a) and no observable luminescence. When ν_l is well into the yellow exciton continuum, relaxation of the photogenerated exciton of the Y-nP levels requires emission of many more phonons. As a result more of the relaxed Y-nP excitons are thermalized and the luminescence from their radiative recombination becomes detectable. When the incident photon energy is such that the photogenerated exciton can relax down to the Y-nP levels by emission of a LO2 phonon plus only a small number of LO1 or Γ^-_{12} phonons, peaks appear in the excitation spectra due to resonant Raman scattering.

ACKNOWLEDGMENTS

This project was started when one of the authors (P.Y.Y) was at the Dept. of Physics, University of California, Berkeley, Calif. We are grateful to Dr. Yve Petroff for generously providing the Cu_2O samples and to J. A. Bradley for expert technical assistance. This research was supported in part by ERDA.

APPENDIX

In this Appendix we present calculations and numerical values of the matrix elements of the Fröhlich Hamiltonian H_{EL} [see Eq. (42) of I][16]:

$$H_{EL}(\mathrm{LO})=Ak^{-1}\left[\exp(ip_e\vec{k}\cdot\vec{r})-\exp(-ip_h\vec{k}\cdot\vec{r})\right], \quad (A1)$$

where

$$A=\left[\frac{2\pi\hbar\omega_{\mathrm{LO}}e^2}{V_0}\left(\frac{1}{\epsilon_\infty}-\frac{1}{\epsilon_0}\right)\right]^{1/2}. \quad (A2)$$

In (A1) and (A2) $\epsilon_0,\epsilon_\infty$ are the static and optical frequency dielectric constants of the crystal, V_0 is the volume of the crystal, k and $\hbar\omega_{\mathrm{LO}}$ are the wave vector and energy of the longitudinal optical phonon, m_e,m_h are the effective masses of the electron and the hole forming the exciton, p_h

$=m_h/(m_e+m_h)$, and $p_e=m_e/(m_e+m_h)$. The matrix elements of H_{EL} we are interested in are $F_{mS,nP}=\langle mS|H_{EL}|nP\rangle$, $F_{mD,nP}=\langle mD|H_{EL}|nP\rangle$, $F_{mS,EP}=\langle mS|H_{EL}|EP\rangle$, and $F_{mD,EP}=\langle mD|H_{EL}|EP\rangle$, where $\langle mS|$ stands for the wave function of an exciton level with principal quantum number m and S orbital symmetry. Similar explanations apply to $\langle mD|$ and $\langle nP|$. $\langle EP|$ denotes an exciton in the continuum with energy E and orbital symmetry P. We shall assume hydrogenic wave functions for the yellow exciton levels in Cu_2O with a Bohr radius,[23]

$$a_0=\hbar^2\epsilon_0/\mu e^2\,, \tag{A3}$$

where the reduced mass μ is given by $\mu^{-1}=m_e^{-1}+m_h^{-1}$.

Calculating the Fröhlich matrix elements is equivalent to calculating the matrix elements of the operators: $\exp(ip_e\vec{k}\cdot\vec{r})$ and $\exp(-ip_h\vec{k}\cdot\vec{r})$. These matrix elements will be denoted by

$$q_e(\vec{k};mD,nP)=\langle mD|e^{ip_e\vec{k}\cdot\vec{r}}|nP\rangle$$

and

$$q_h(\vec{k};mD,nP)=\langle mD|e^{-ip_h\vec{k}\cdot\vec{r}}|np\rangle\,.$$

We will present both analytic expressions and numerical values for $F_{mS,nP}(k)$ and $F_{mD,nP}(k)$ but only numerical values for $F^{(1)}_{mS,EP}$ and $F^{(1)}_{mD,EP}$ for two values of E of interest to us (deduced from Ref. 17). Analogous Fröhlich matrix elements of the form $\langle nS|H_{EL}|mS\rangle$ and $\langle nS|H_{EL}|ES\rangle$ can be found in Ref. 24.

1. $F_{mS,nP}(k)$ and $F_{mD,nP}(k)$

$$F_{mS,nP}(k)=Ak^{-1}[q_e(k;mS,nP)-q_h(k;mS,nP)] \tag{A4}$$

$$q_e(k;mS,nP)=\frac{4\sqrt{3}\,(m-1)!\,[(n-2)!\,(n+1)!\,]^{1/2}}{n^3m^{3/2}}(ip_eka_0)$$
$$\times\sum_{s=0}^{m-1}\sum_{t=0}^{n-2}\frac{(-2)^{s+t}(mn)^{s+t+5}I_{s+t+3}[ip_eka_0mn/(m+n)]}{m^sn^t(m+n)^{s+t+5}(m-1-s)!\,(1+s)!\,s!\,(n-t-2)!\,t!\,(t+3)!}\,. \tag{A5}$$

The function $I_l(x)$ (l being an integer) is defined as

$$I_l(x)=\frac{2(l-1)!}{(1-x^2)^l}\sum_{i=1}^{\lambda-1}\left({}_lC_{2i}+\frac{{}_{l-1}C_{2i-1}-{}_{l-1}C_{2i+1}}{l-1}\right)x^{2(i-1)}+\frac{2(l-1)!}{(1-x^2)^l}x^{2(l-1)}\times\begin{cases}1+l & \text{if } l=2\lambda+1\\ l(l+1)^{-1} & \text{if } l=2\lambda\,,\end{cases} \tag{A6}$$

where ${}_iC_j$ denotes the binomial coefficients. $q_h(k;mS,nP)$ can be obtained from $q_e(k;mS,nP)$ by replacing ip_e by $-ip_h$ whenever it occurs. Similarly,

$$F_{mD,nP}(k)=Ak^{-1}[q_e(k;mD,nP)-q_h(k;mD,nP)]\,, \tag{A7}$$

$$q_e(k;mD,nP)=\frac{48\sqrt{5}}{m^4n^3}(ip_eka_0)[(m-3)!\,(m+2)!\,(n-2)!\,(n+1)!\,]^{1/2}$$
$$\times\sum_{s=0}^{m-3}\sum_{t=0}^{n-2}\frac{(-2)^{s+t}(mn)^{s+t+7}}{m^sn^t(m-3-s)!\,(n-2-t)!s!\,t!\,(s+5)!\,(t+3)!\,(m+n)^{s+t+7}}$$
$$\times\left[\left(1-\frac{1}{2\sqrt{3}}\right)I_{s+t+5}\left(\frac{ip_eka_0mn}{m+n}\right)+\left(\frac{3}{2\sqrt{3}}-1\right)J_{s+t+5}\left(\frac{ip_eka_0mn}{m+n}\right)\right]. \tag{A8}$$

The function $J_l(\chi)$ is defined by

$$J_l(\chi)=\frac{2(l-1)!}{(1-\chi^2)^l\chi^2}\left[1+\sum_{i=1}^{\lambda}{}_lC_{2i}\chi^{2i}-\frac{3(1-\chi^2)}{l-1}\left(1+\sum_{i=1}^{\lambda-1}{}_{l-1}C_{2i+1}\chi^{2i}\right)\right]$$
$$+\frac{12(l-3)!}{(1-\chi^2)^{l-2}\chi^4}\left[1+\sum_{i=1}^{\lambda-1}{}_{l-2}C_{2i}\chi^{2i}-\frac{1-\chi^2}{l-3}\left(1+\sum_{i=1}^{\lambda-2}{}_{l-3}C_{2i+1}\chi^{2i}\right)\right]. \tag{A9}$$

Using Eqs. (A4)–(A9) we can calculate the matrix elements $F_{mS,nP}(k)$ and $F_{mD,nP}(k)$ for any phonon wave vector k. In Tables II-IV we list numerical values of some of the Fröhlich matrix elements of LO1 and LO2 relevant to this paper. In calculating these tables we used $m_e=0.61m_0$ (mass of free electron) and $m_h=0.84m_0$ measured by Zhilich *et al.*[25,26]

2. $F_{mS,EP}(k=0)$ and $F_{mD,EP}(k=0)$

The evaluation of Fröhlich matrix elements between discrete exciton levels and continuum states

for nonzero wave vectors is very tedious. On the other hand, if we neglect the phonon wave vector we find that $F_{mS,EP}(0) = (iA)(1/\sqrt{3}\ 2\pi)\langle mS|r|EP\rangle$ and

$$F_{mD,EP}(0) = (iA)3\sqrt{5}/4\pi[\tfrac{2}{3}(1-1/2\sqrt{3})+\tfrac{2}{5}(\sqrt{3}/2-1)] \times\langle mD|r|EP\rangle ,$$

where $\langle mS|r|EP\rangle$ and $\langle mD|r|EP\rangle$ have already been evaluated to a high degree of accuracy by a number of authors.[17]

In Table V we list the numerical values of $F^{(1)}_{mD,EP}$ and $F^{(1)}_{mS,EP}$ for two particular values of E: $E/2\pi\hbar c = 17\,592$ and $17\,720$ cm^{-1}. In terms of the parameter $\epsilon' = (E-\hbar\omega_{Y\infty})/$(yellow-exciton Rydberg) in Ref. 17, these two values of E correspond to $\epsilon' = 0.085$ and 0.25 Ry, respectively. They were chosen such that when $\hbar\omega_l = E$ the scattered photons for the 2LO1 mode are resonant with the Y-$2P$ and Y-$3P$ levels.

[1] A. Compaan and H. Z. Cummins, Phys. Rev. Lett. 31, 41 (1973).
[2] A. Z. Genack, H. Z. Cummins, M. A. Washington, and A. Compaan, Phys. Rev. B 12, 2478 (1975).
[3] M. A. Washington, A. Z. Genack, H. Z. Cummins, R. H. Bruce, A. Compaan, and R. A. Forman, Phys. Rev. B 15, 2145 (1977).
[4] P. Y. Yu, Y. R. Shen, and Y. Petroff, Solid State Commun. 12, 973 (1973).
[5] P. F. Williams and S. P. S. Porto, Phys. Rev. B 8, 1782 (1973).
[6] A. Compaan, Solid State Commun. 16, 293 (1975).
[7] P. Y. Yu and Y. R. Shen, Phys. Rev. B 12, 1377 (1975).
[8] P. Y. Yu and Y. R. Shen, Phys. Rev. Lett. 32, 373 (1974).
[9] S. Nikitine, in *Optical Properties of Solids*, edited by S. Nudelman and S. S. Mitra (Plenum, New York, 1969).
[10] A. Daunois, J. L. Diess, J. C. Merle, C. Wecker, and S. Nikitine, in *Eleventh International Conference on the Physics of Semiconductors, Warsaw, 1972* (State Publishing House, Warsaw, 1973), p. 1402; J. L. Diess and A. Daunois, Surf. Sci. 37, 804 (1973).
[11] Y. Petroff, P. Y. Yu, and Y. R. Shen, Phys. Rev. B 12, 2488 (1975).
[12] P. Y. Yu and J. E. Smith, Jr., Phys. Rev. Lett. 37, 622 (1976).
[13] R. Loudon, Proc. R. Soc. A 275, 218 (1963).
[14] P. Y. Yu and Y. R. Shen, Phys. Rev. Lett. 29, 468 (1972); and W. Richter, in *Springer Tracts in Modern Physics* (Springer-Verlag, New York, 1977), Vol. 78.
[15] Y. Toyozawa, J. Phys. Chem. Solids 25, 59 (1964).
[16] Y. Toyozawa, Prog. Theor. Phys. 20, 53 (1958).
[17] See, for example, G. Peach, Mem. R. Astron. Soc. 71, 13 (1967), and references therein.
[18] J. L. Birman, Phys. Rev. B 9, 4518 (1974).
[19] R. M. Martin and C. M. Varma, Phys. Rev. Lett. 26, 1241 (1971).
[20] R. M. Martin and T. C. Damen, Phys. Rev. Lett. 26, 86 (1971).
[21] T. Ueno, J. Phys. Soc. Jpn. 26, 438 (1969).
[22] A. Compaan and H. Z. Cummins, Phys. Rev. B 6, 4753 (1972).
[23] See, for example, L. Pauling and E. B. Wilson, *Introduction to Quantum Mechanics* (McGraw-Hill, New York, 1935).
[24] P. F. Williams, Ph.D. thesis (University of Southern California, 1973) (unpublished).
[25] A. G. Zhilich, J. Halpern, and B. P. Zakhavchenya, Phys. Rev. 188, 1294 (1969).
[26] J. W. Hodby, T. E. Jenkins, C. Schwab, H. Tamura, and D. Trivich, J. Phys. C 9, 1429 (1976). Using cyclotron resonance these authors obtained $m_e = 0.99m_0$ and $m_h = 0.69m_0$ instead.